

## REPORTS

## FRUSTRATED MAGNETISM

Hidden order in spin-liquid  $\text{Gd}_3\text{Ga}_5\text{O}_{12}$ Joseph A. M. Paddison,<sup>1,2,3</sup> Henrik Jacobsen,<sup>4,5</sup> Oleg A. Petrenko,<sup>6</sup> Maria Teresa Fernández-Díaz,<sup>7</sup> Pascale P. Deen,<sup>4,5\*</sup> Andrew L. Goodwin<sup>1\*</sup>

Frustrated magnetic materials are promising candidates for new states of matter because lattice geometry suppresses conventional magnetic dipole order, potentially allowing “hidden” order to emerge in its place. A model of a hidden-order state at the atomic scale is difficult to deduce because microscopic probes are not directly sensitive to hidden order. Here, we develop such a model of the spin-liquid state in the canonical frustrated magnet gadolinium gallium garnet ( $\text{Gd}_3\text{Ga}_5\text{O}_{12}$ ). We show that this state exhibits a long-range hidden order in which multipoles are formed from 10-spin loops. The order is a consequence of the interplay between antiferromagnetic spin correlations and local magnetic anisotropy, which allows it to be indirectly observed in neutron-scattering experiments.

When a material undergoes a transition to an ordered state, its physical properties change. One of the greatest triumphs of 20th-century physics was to explain these macroscopic changes in terms of the microscopic ordering of atoms and magnetic dipole moments (spins). A canonical example is antiferromagnetic order, which remained hidden until the development of neutron-scattering experiments in the 1940s (1). Today, a similar situation exists in “hidden order” materials, where the order is a type that cannot be directly probed by our current experimental techniques [see, e.g., (2–4)]. Exotic hidden-order states such as quantum spin nematics, chiral spin ices, and multipolar spin-orbital order have been theoretically proposed (5–7). Experimentally, the canonical example of a hidden-order state is the material  $\text{URu}_2\text{Si}_2$  (2, 8).

Frustrated magnetic materials are promising candidates for the discovery of hidden-order states (9). In frustrated systems, the lattice geometry suppresses conventional (long-range) spin order and a “spin liquid” phase may exist instead (10). Crucially, the strong spin correlations in spin-liquid states can lead to spin clusters behaving as a single object. Even though individual spins remain in a liquid-like state (11), spin clusters may have properties that exhibit nondipolar long-range order. The experimental signature of a potential hidden-order state is an anomaly in thermodynamic measurements that is not accompanied by a transition to long-range or frozen spin order (indicated, e.g., by the development of magnetic Bragg peaks in neutron-diffraction experiments) (2). This anomaly may be either sharp, as in a conventional

second-order phase transition, or broad, as for the transition from the paramagnetic phase to the “Coulomb phase” in spin-ice materials (12).

The well-studied frustrated magnet  $\text{Gd}_3\text{Ga}_5\text{O}_{12}$  [gadolinium gallium garnet (GGG)] exhibits thermodynamic anomalies of the second type. In GGG, a spin-liquid state is observed at temperatures above a spin-glass transition at  $T_g \approx 0.14$  K (13). Evidence for a conventional spin liquid in GGG is the suppression of  $T_g$  to temperatures far below the antiferromagnetic interaction strength of  $\sim 2$  K (14–16), the observation of liquid-like magnetic diffuse scattering in powder neutron-scattering measurements (17), and the persistence of strong spin fluctuations to low temperature (18–20). Yet, broad anomalies are present in both the nonlinear susceptibility  $\chi_3$  and the magnetic specific heat at around 0.5 K, which do not yet have a well-understood microscopic origin (13, 21).

The crystal structure of GGG is shown in Fig. 1A. The unit cell is cubic and contains 24 equivalent magnetic  $\text{Gd}^{3+}$  ions with spin quantum number  $S = 7/2$ . The  $\text{Gd}^{3+}$  ions form two interpenetrating networks of opposite chirality, each of which describes a three-dimensional arrangement of corner-sharing triangles known as hyperkagome. The local environment of the  $\text{Gd}^{3+}$  ions is shown in Fig. 1B, where local axes  $x$ ,  $y$ , and  $z$  are defined by the three twofold rotational axes of point symmetry (table S1) (22). Of particular importance in the GGG structure are the 10-spin loops shown in blue in Fig. 1B, which are the shortest path connecting a  $\text{Gd}^{3+}$  ion back to itself beyond individual triangles. Each  $\text{Gd}^{3+}$  sits in the middle of exactly one loop; hence, loop and atom share the same point symmetry and the local axes defined for atoms apply equally to loops. In a simple model, which considers only nearest-neighbor antiferromagnetic interactions, collective rotations of the loop spins allow the system to move at no energy cost between its degenerate ground states (23). We therefore anticipate that the 10-spin loops should play a key role in any emergent behavior present in the spin-liquid state.

We performed single-crystal neutron-scattering measurements on GGG in order to probe the spin-

liquid state. These measurements are challenging because of the very large neutron absorption cross section of natural Gd, and a high-energy incident neutron beam was used to mitigate against this problem (22). The left-hand panels of Fig. 2A show single-crystal neutron-scattering data at  $T = 0.175$  K. To model these highly structured magnetic diffuse-scattering data, we use the reverse Monte Carlo (RMC) method (24, 25) to perform quantitative refinement to magnetic diffuse-scattering data from (17), which were collected on a powder sample (fig. S1) (22). The RMC method has two important properties: It generates an atomic-scale model from which arbitrary (nondipolar) correlation functions can be calculated, and it does not introduce a predetermined set of magnetic interactions that could bias the results (26). Excellent agreement between the RMC fit and the powder data is achieved at  $T = 0.175$  K (Fig. 2B). Calculations of the single-crystal scattering from the refined RMC model show close qualitative agreement with the experimental single-crystal data, which provides evidence for the validity of the RMC model (Fig. 2A, right panels). Consistent with Mössbauer measurements (27), we obtain a strongly anisotropic distribution of spin orientations with spins preferentially oriented within their local  $xy$  planes (Fig. 2B, inset, and fig. S2). Our RMC refinements do not determine the term in the Hamiltonian responsible for this  $xy$  anisotropy. However, additional simulations of a spin Hamiltonian for GGG (15, 16) showed that the magnetic dipolar interaction (which couples spin and space degrees of freedom) generates the same  $xy$  anisotropy [fig. S7) (22). The sensitivity of the powder-averaged data to local spin anisotropy was confirmed by showing that an isotropic model does not fit the data successfully (green line in Fig. 2B). Consistent with simulations (28), the radial spin correlation function  $\langle \mathbf{S}(0) \cdot \mathbf{S}(r) \rangle$  reveals a rapid decay of spin correlations with an exponential correlation length  $\xi = 4.951(2)$  Å (similar to the nearest-neighbor distance  $r_{\text{nn}} = 3.78$  Å) and a nearest-neighbor spin correlation coefficient  $\langle \mathbf{S}(0) \cdot \mathbf{S}(r_{\text{nn}}) \rangle$  close to  $-0.5$  (Fig. 2C) (angle brackets denote a configurational average). The temperature dependence of  $\xi$  was obtained from fits to powder diffuse scattering data at higher temperatures (22) and shows a gradual decrease with increasing temperature (Fig. 2C, inset). Based on this analysis, we conclude that the spin anisotropy and short-range dipole order of our model are consistent with expectations.

To look for exotic behavior beyond dipole order, we consider the 10-ion loops that are shown in Fig. 3A. Adjacent spins in a loop are nearest neighbors and are therefore antiferromagnetically correlated. Surprisingly, inspection of spin configurations suggested that strong antiferromagnetic alignment persists beyond nearest neighbors and throughout the loop, a result obscured by the radial average in Fig. 2C. To quantify this correlation, we calculate from our RMC configurations the average spin alignment axis of each loop (22),

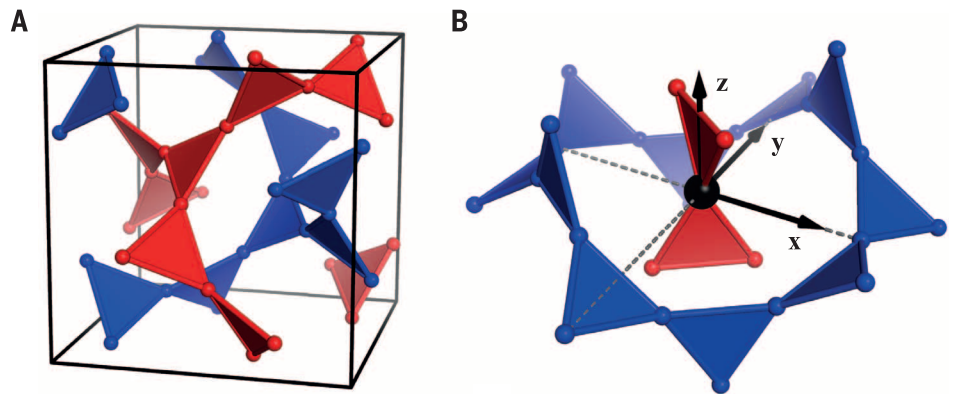
$$\mathbf{L}(r) = \frac{1}{10} \sum_n \cos(n\pi) \mathbf{S}_n(r), \quad (1)$$

<sup>1</sup>Department of Chemistry, University of Oxford, Inorganic Chemistry Laboratory, South Parks Road, Oxford OX1 3QR, UK. <sup>2</sup>ISIS Facility, Rutherford Appleton Laboratory, Chilton, Didcot, Oxfordshire OX11 0QX, UK. <sup>3</sup>School of Physics, Georgia Institute of Technology, Atlanta, GA 30332, USA. <sup>4</sup>Nanoscience Center, Niels Bohr Institute, University of Copenhagen, DK-2100 Copenhagen Ø, Denmark. <sup>5</sup>European Spallation Source, Tunavägen 24, Lund, Sweden. <sup>6</sup>Department of Physics, University of Warwick, Coventry, CV4 7AL, UK. <sup>7</sup>Institut Max von Laue–Paul Langevin, F-38042 Grenoble 9, France.

\*Corresponding author. E-mail: pascale.deen@esss.se (P.P.D.); andrew.goodwin@chem.ox.ac.uk (A.L.G.)

**Fig. 1. Crystallographic properties of GGG.**

(A) Crystal structure of GGG, showing only magnetic  $\text{Gd}^{3+}$  ions. The two interpenetrating networks of corner-sharing triangles are colored red and blue. (B) Local environment of  $\text{Gd}^{3+}$  ions. The local axes  $x$ ,  $y$ , and  $z$  are defined by the three twofold axes of point symmetry of the  $\text{Gd}^{3+}$  site:  $x \in (100)$  and  $y, z \in \frac{1}{\sqrt{2}}(110)$ , where  $z$  is chosen to pass through the centers of the two triangles that contain the  $\text{Gd}^{3+}$  ion. Each  $\text{Gd}^{3+}$  ion is located at the center of a loop of 10  $\text{Gd}^{3+}$  ions from the other network, where the mean plane of the loop is perpendicular to the local  $z$  axis.



where  $\mathbf{r}$  is the position of the center of the loop and  $\mathbf{S}_n$  are unit-length spins within the loop ( $n \in \{1, \dots, 10\}$ ). We refer to  $\mathbf{L}(\mathbf{r})$  as the “10-spin director” to emphasize that  $\mathbf{L}$  does not transform as a vector, because the twofold symmetry of the  $\text{Gd}^{3+}$  site requires that both  $\mathbf{L}(\mathbf{r})$  and  $-\mathbf{L}(\mathbf{r})$  identify the same alignment axis [our use of the director here mirrors the description of nematic liquid crystals (29)]. The average magnitude  $\langle |\mathbf{L}(\mathbf{r})| \rangle = 0.49$  with standard deviation 0.18, which shows that antiferromagnetic correlation is strong within each loop and relatively consistent between different loops. The cyclic arrangement of 10 antiferromagnetic spins in a ring describes a multipole of order 6, which contains five nodal planes orthogonal to the plane of the loop and a single nodal plane coincident with it (Fig. 3A). Viewed in these terms, the normalized 10-spin director  $\hat{\mathbf{L}} = \mathbf{L}/|\mathbf{L}|$  describes the multipole orientation associated with a given 10-ion loop. Figure 3B shows our key result: the distribution of normalized 10-spin directors is strongly peaked along the local  $z$  axis.

This result is notable because it shows that the fluctuations of the 10 spins in a loop select a single axis on average, so the rotational degree of freedom possessed by  $xy$ -like spins is lost in the loop directors. Hence, the 10-spin directors have no ground-state degrees of freedom and are ordered, with excitations normal to the local  $z$  axis (Fig. 3B). Moreover, because the 10-spin directors describe multipole orientations, the order is multipolar. The unit cell of this magnetic multipole crystal is shown in Fig. 3C. The multipole order preserves the symmetry of the crystal structure but is not required by this symmetry, which only constrains the distribution of 10-spin directors to preserve the three twofold rotation axes. Figure 3D shows the axial correlation function of the normalized 10-spin directors extracted from our RMC configurations (22),

$$g_L(r) = 2\langle |\hat{\mathbf{L}}(0) \cdot \hat{\mathbf{L}}(r)| \rangle - 1 \quad (2)$$

which is equal to  $-1$  if, on average, loop directors separated by distance  $r$  are orthogonal to each other and to  $+1$  if they are collinear. The correlation length of this function diverges within the statistical error of our refinements (22), as is to be expected from the axial distribution of 10-spin directors in Fig. 3B. Analogous to a noncollinear antiferromagnet, the noncollinearity of local  $z$  axes for different loops leads to  $g_L(r)$

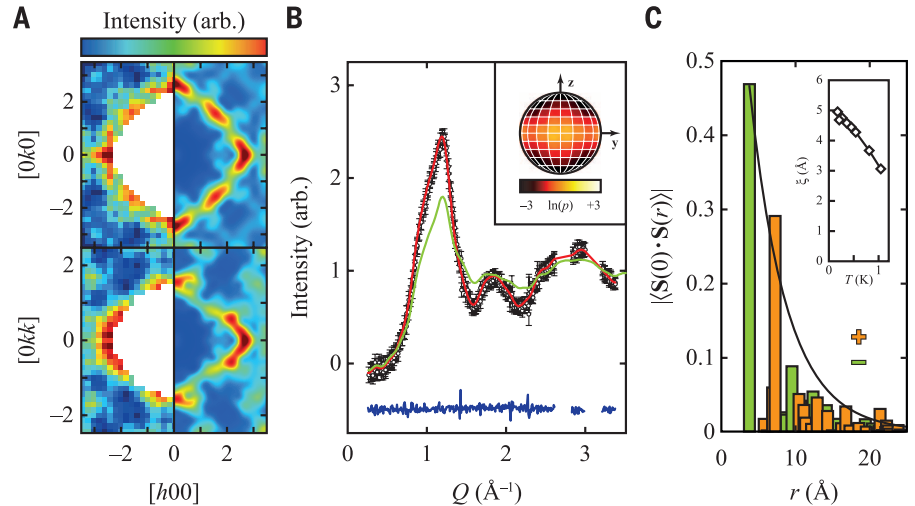


**Fig. 2. Experimental data, fits, and calculations for GGG at  $T = 0.175$  K.** (A) Single-crystal magnetic diffuse scattering in two reciprocal-space planes. The upper image shows the  $(hk0)$  plane, and the lower image shows the  $(hkk)$  plane. In each image, the left panel shows experimental data and the right panel shows the calculation from RMC refinements described in the text. Regions where there are no data are shown in white. (B) RMC fit to powder diffuse-scattering data [from (17)]. Data are shown as black circles, fit as a red line, and difference (fit – data) as a blue line. The scattering function calculated from the alternative isotropic model described in the text is shown as a green line. The inset shows a stereographic projection of the logarithmic probability distribution  $\ln(\rho)$  of spin orientations [defined in (22)], revealing preferential spin alignment in the local  $xy$  plane (Fig. 1B). (C) Radial spin correlation function obtained from our RMC configurations. The bars show spin correlation values, and the solid black line shows a fit to an exponential envelope,  $\pm \exp(-r/\xi)$ , where  $\xi = 4.951(2)$  Å. Correlations with positive (ferromagnetic) values are shown in orange, and correlation with negative (antiferromagnetic) values are shown in green. The inset shows the temperature dependence of  $\xi$  (the solid line is a guide to the eye). Error bars in (C) are smaller than the line thickness or symbol size in the plots.

taking several values but does not affect the divergence of the correlation length (fig. S3).

How is our analysis sensitive to nondipolar order, given that neutron scattering is a dipolar probe? To answer this question, we note that neutron scattering is directly sensitive to two quantities: the spin anisotropy and the spin-pair correlations (30). If an interplay of both quantities generates hidden order, neutron scattering may be indirectly sensitive to the hidden order itself. We performed Monte Carlo simulations, which show that this is the case for GGG: Long-range multipole order is present when both  $xy$  anisotropy and antiferromagnetic interactions are included but is absent for either (i) isotropic antiferromagnetic interactions or (ii) noninteracting spins with  $xy$  anisotropy [figs. S5 and S8] (22). Hence, hidden

order is not a consequence of either  $xy$  anisotropy or antiferromagnetic interactions alone.

The development of hidden order provides a plausible explanation for observed thermodynamic anomalies in the spin-liquid state of GGG. We show this by considering a simple model in which spins are constrained to lie in their local  $xy$  planes and are coupled by antiferromagnetic nearest-neighbor interactions. We do not claim that this  $xy$  model accurately represents the spin Hamiltonian of GGG but consider it instead because it is the simplest model showing the hidden-order state. From this model, we calculate two quantities: the magnetic specific heat  $C_{\text{mag}}$  and a limiting multipole correlation  $g_{\text{max}}$ , which we determine by fitting a straight line to  $g_L(r)$  at the distances where it takes its maximum value

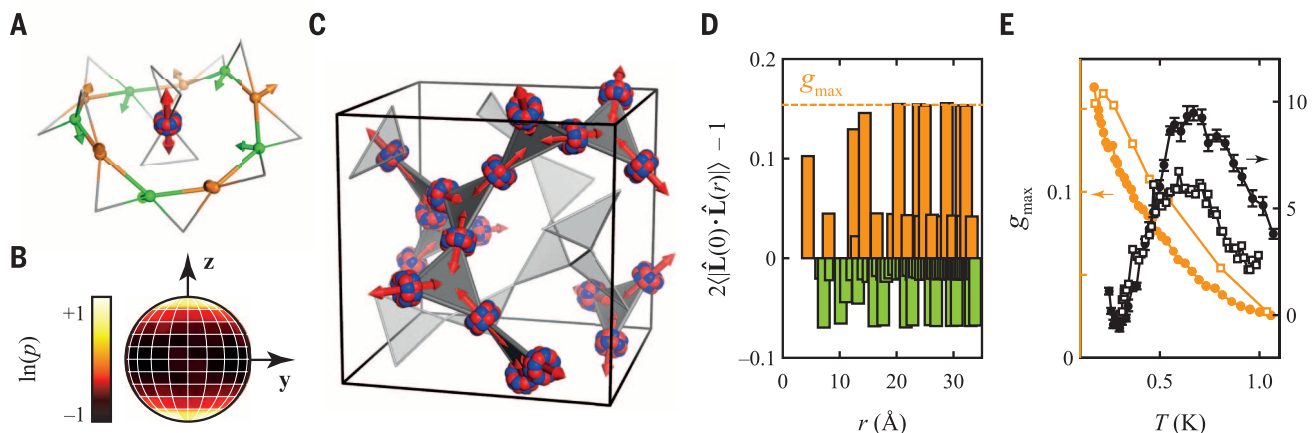


**Fig. 3. Multipole order in GGG.** (A) Relationship between representative spin orientations and 10-spin director for a 10-spin loop. Antiferromagnetically correlated spins are colored alternating green and orange as the loop is traversed. The multipole formed by the 10 spins is shown at the center of the loop, and the 10-spin director defined in the text is shown as a red double-headed arrow. (B) Stereographic projection showing that the logarithmic probability distribution function  $\ln(p)$  [defined in (22)] of normalized 10-spin directors extracted from our RMC configurations (22) is strongly peaked along the local  $z$  axis [shown by the red double-headed arrow in (A)]. Fluctuations of the loop director normal to  $z$  are also apparent. (C) Crystal structure showing the unit cell of the magnetic multipole crystal. Multipoles and 10-spin directors are shown as in (A) and are illustrated for only one of the two networks for clarity. (D) Axial correlation func-

tion of normalized 10-spin directors calculated from our RMC configurations (22), showing the presence of long-range multipole order. Collinear correlations are shown as orange bars, and orthogonal correlations are shown as green bars. (E) Temperature evolution of the broad peak in the magnetic specific heat  $\Delta C$  (black symbols) compared with temperature evolution of the limiting multipole correlation  $g_{\max}$  (orange symbols). Open squares show experimental specific-heat data [from (13)] and  $g_{\max}$  obtained from RMC refinement to experimental neutron-scattering data, whereas solid circles show specific heat and  $g_{\max}$  calculated for a model with antiferromagnetic nearest-neighbor interactions and  $xy$  anisotropy as described in the text. The broad specific-heat peak has been isolated by fitting polynomial background functions to the experimental specific-heat data and model calculation (22).

for the multipole crystal—i.e., the distances separating loops that share the same local axes (Fig. 3D). Figure 3E compares the broad peak in the specific heat and  $g_{\max}$  determined from the  $xy$  model with the experimental specific-heat peak and  $g_{\max}$  determined from RMC refinement. We make three key observations. First, a broad specific-heat peak occurs in the  $xy$  model and the real material, which both show hidden order; moreover, this specific-heat peak is absent for models without hidden order (fig. S6) (22). Second, there is a large change in  $g_{\max}$  over the temperature range where the specific-heat peak develops but only a much smaller change in the spin correlation length (Fig. 2C, inset). Third, the temperature evolution of the specific-heat peak correlates with the evolution of hidden order in a similar way for both  $xy$  model and experiment (Fig. 3E). These results suggest that the broad specific-heat anomaly is a signature of loss of entropy associated with the developing hidden order.

The hidden-order state that we propose for GGG does not break the crystal symmetry and is built from groups of spins that are individually fluctuating in space and time (18–20); for examples of how spin fluctuations occur consistently with multipolar order, see fig. S4 (22). It is also likely that the multipolar order will be apparent in larger clusters than the 10-spin loops. Compared with  $\text{URu}_2\text{Si}_2$  (2), the lack of symmetry-breaking in GGG broadens the specific-heat anomaly observed as the hidden-order state develops, similar to the transition to the Coulomb phase in spin-ice materials (12). An interesting comparison can be drawn with frustrated spinels such as  $\text{MgCr}_2\text{O}_4$ , in which hexagonal spin loops can form strongly ordered (“protected”) degrees

of freedom but adjacent loops are only weakly correlated (31, 32). The hidden order in GGG represents the opposite limit, in which the loops are long-range ordered, whereas individual spins show only short-range correlations. The hidden order in GGG therefore has properties fundamentally different from previous examples. Our results suggest that the atomic-scale refinement approach used here will prove valuable to unmask hidden-order states in other materials, such as chiral-spin liquids in frustrated magnetic materials (11) and spin nematics in high-temperature superconductors (33).

#### REFERENCES AND NOTES

- C. G. Shull, J. S. Smart, *Phys. Rev.* **76**, 1256–1257 (1949).
- J. A. Mydosh, P. M. Oppeneer, *Rev. Mod. Phys.* **83**, 1301–1322 (2011).
- P. Santini, S. Carretta, N. Magnani, G. Amoretti, R. Ciachuffo, *Phys. Rev. Lett.* **97**, 207203 (2006).
- S. Chakravarty, R. B. Laughlin, D. K. Morr, C. Nayak, *Phys. Rev. B* **63**, 094503 (2001).
- P. Chandra, P. Coleman, *Phys. Rev. Lett.* **66**, 100–103 (1991).
- S. Onoda, Y. Tanaka, *Phys. Rev. Lett.* **105**, 047201 (2010).
- H. Ikeda *et al.*, *Nat. Phys.* **8**, 528–533 (2012).
- E. Ressouche *et al.*, *Phys. Rev. Lett.* **109**, 067202 (2012).
- J. T. Chalker, P. C. W. Holdsworth, E. F. Shender, *Phys. Rev. Lett.* **68**, 855–858 (1992).
- R. Moessner, A. P. Ramirez, *Phys. Today* **59**, 24–29 (2006).
- Y. Machida, S. Nakatsuji, S. Onoda, T. Tayama, T. Sakakibara, *Nature* **463**, 210–213 (2010).
- R. G. Melko, M. J. P. Gingras, *J. Phys. Condens. Matter* **16**, R1277–R1319 (2004).
- P. Schiffer *et al.*, *Phys. Rev. Lett.* **74**, 2379–2382 (1995).
- W. Kinney, W. Wolf, *J. Appl. Phys.* **50** (B3), 2115 (1979).
- T. Yavorskii, M. Enjalran, M. J. P. Gingras, *Phys. Rev. Lett.* **97**, 267203 (2006).
- N. d’Ambrumenil, O. A. Petrenko, H. Mutka, P. P. Deen, *Phys. Rev. Lett.* **114**, 227203 (2015).
- O. A. Petrenko, C. Ritter, M. Yethiraj, D. McK. Paul, *Phys. Rev. Lett.* **80**, 4570–4573 (1998).
- P. P. Deen *et al.*, *Phys. Rev. B* **82**, 174408 (2010).
- I. M. Marshall *et al.*, *J. Phys. Condens. Matter* **14**, L157–L163 (2002).

- S. R. Dunsiger *et al.*, *Phys. Rev. Lett.* **85**, 3504–3507 (2000).
- J. A. Quilliam *et al.*, *Phys. Rev. B* **87**, 174421 (2013).
- Materials and methods are available as supporting materials on Science Online.
- S. Ghosh, T. F. Rosenbaum, G. Aeppli, *Phys. Rev. Lett.* **101**, 157205 (2008).
- R. L. McGreevy, L. Pusztai, *Mol. Simul.* **1**, 359–367 (1988).
- J. A. M. Paddison, A. L. Goodwin, *Phys. Rev. Lett.* **108**, 017204 (2012).
- J. A. M. Paddison, J. R. Stewart, A. L. Goodwin, *J. Phys. Condens. Matter* **25**, 454220 (2013).
- P. Bonville, J. A. Hodges, J. P. Sanchez, P. Vulliet, *Phys. Rev. Lett.* **92**, 167202 (2004).
- O. A. Petrenko, D. McK. Paul, *Phys. Rev. B* **63**, 024409 (2000).
- R. W. Ruhwandel, E. M. Terentjev, *Phys. Rev. E* **56**, 5561–5565 (1997).
- G. L. Squires, *Introduction to the Theory of Thermal Neutron Scattering* (Cambridge University Press, Cambridge, 1978).
- S.-H. Lee *et al.*, *Nature* **418**, 856–858 (2002).
- K. Tomiyasu *et al.*, *Phys. Rev. Lett.* **110**, 077205 (2013).
- C. V. Parker *et al.*, *Nature* **468**, 677–680 (2010).

#### ACKNOWLEDGMENTS

We thank S. A. Hall, M. E. Zhitomirsky, N. d’Ambrumenil, J. R. Stewart, M. J. P. Gingras, T. Yavorskii, S. E. Dutton, M. Mourigal, M. Evans, W. J. K. Fletcher, and M. J. Cliffe for useful discussions; O. Young and S. Holm for assistance with the early experimental work; and the staff at the Institut Max von Laue–Paul Langevin for experimental support. P.P.D. and H.J. gratefully acknowledge financial support from the Danish Research Council for Nature and Universe through DANSCATT. J.A.M.P. and A.L.G. gratefully acknowledge financial support from the STFC, EPSRC (EP/G004528/2), and ERC (279705). The experimental data collected in this study are available as supplementary materials.

#### SUPPLEMENTARY MATERIALS

www.sciencemag.org/content/350/6257/179/suppl/DC1  
Materials and Methods  
Supplementary Text  
Figs. S1 to S8  
Table S1  
Data Files S1 to S3  
References (34–43)

19 December 2014; accepted 4 August 2015  
10.1126/science.aaa5326

---

*This copy is for your personal, non-commercial use only.*

---

**If you wish to distribute this article to others**, you can order high-quality copies for your colleagues, clients, or customers by [clicking here](#).

**Permission to republish or repurpose articles or portions of articles** can be obtained by following the guidelines [here](#).

**The following resources related to this article are available online at [www.sciencemag.org](http://www.sciencemag.org) (this information is current as of October 8, 2015):**

**Updated information and services**, including high-resolution figures, can be found in the online version of this article at:

<http://www.sciencemag.org/content/350/6257/179.full.html>

**Supporting Online Material** can be found at:

<http://www.sciencemag.org/content/suppl/2015/10/07/350.6257.179.DC1.html>

This article **cites 41 articles**, 1 of which can be accessed free:

<http://www.sciencemag.org/content/350/6257/179.full.html#ref-list-1>

This article appears in the following **subject collections**:

Physics

<http://www.sciencemag.org/cgi/collection/physics>